SWOT support within GAMMA Software

Urs Wegmüller, Christophe Magnard, Gamma Remote Sensing AG

Version 26-Nov-2024 (initial version)

1. INTRODUCTION

In this document, the support provided in the GAMMA Software for the processing of data of the SWOT mission is summarized. The **Surface Water and Ocean Topography (SWOT)** mission is a joint collaboration between the National Aeronautics and Space Administration NASA, USA, the French Space Agency CNES, the Canadian Space Agency, CSA, and the United Kingdom Space Agency, UKSA, and was launched on Dec. 16, 2022. One of the instruments on SWOT is a Ka-band Radar Interferometer (KaRIn). As the primary instrument of the mission, KaRIn is a near-nadir viewing interferometric altimeter, consisting of two distinct 50 km swaths. It uses two SAR antennas, which are located at the opposite ends of a 10 m boom, enabling researchers to gather information along a roughly 120 km wide swath of the Earth's surface and to discern currents and eddies as small as 20 km across. KaRIn bounces radar pulses off the water's surface and receives the return signal with its antennas at the same time. While the nadir altimeter will point straight down and take data in one dimension, the KaRIn antennas are scanning the surface in two dimensions and collecting data with greater precision than the nadir altimeter alone. Further information on the mission concept is available from https://www.eoportal.org/satellite-missions/swot#spacecraft

An SLC product is available for the KaRIn instrument. This product is called the Level 1B Ka-band Radar Interferometer (KaRIn) high rate (HR) single look complex (SLC) data product from the Surface Water Ocean Topography (SWOT) mission. The KaRIn L1B_HR_SLC data product is defined in the related Product Description Document (JPL D-56410, Revision B, "SWOT Product Description Document: Level 1B KaRIn High Rate Single Look Complex (L1B_HR_SLC) Data Product," Jet Propulsion Laboratory Internal Document, 2023.), available at https://podaac.jpl.nasa.gov/dataset/SWOT_L1B_HR_SLC_2.0

SWOT KaRIn data can be accessed from https://search.earthdata.nasa.gov/search.

The GAMMA Software program *par_SWOT_SLC* supports reading the SWOT KaRIn SLC data.

The importing of the SWOT KaRIn SLC data is described in Section 2, followed by an assessment of the data characteristics, in Section 3. In Section 4, the bistatic-static DInSAR processing sequence is presented followed by a discussion of generated results. The main generated results are a terrain height correction relative to a pre-existing DEM, the single-pass InSAR coherence and the backscatter.

2. SWOT SLC DATA

2.1. Importing SLC data

The SWOT KaRIn SLC data is stored in NetCDF format (*.nc files). Along with the SLC data, associated metadata is provided, including orbit data, DEM heights used in back-projection processing, radiometric calibration details, and noise information.

The noise information was found to be empty for the data investigated.

A SWOT KaRIn acquisition consists of 4 SLCs: a mono-static - bi-static SLC pair in right looking geometry (with a spatial baseline of about 10m, and incidence angles up to about 6 degrees), and a mono-static - bi-static SLC pair in left looking geometry (again with a spatial baseline of about 10m, and incidence angles up to about 6 degrees).

Separate metadata, including orbit data, is provided for each SLC dataset.

The SLCs are provided in skewed slant range geometry. The mono-static and bi-static SLC pair (acquired in the same look direction) are provided in the identical geometry (already co-registered). The Doppler Centroid deviates significantly from zero – as a consequence the azimuth spectrum is not centered, which has to be considered when resampling the data.

A time-domain back-projection processing method is used, which considers a digital elevation model and corrects the data for the related orbit phase (topographic phase). Consequently, the phase of the single-pass interferogram is almost flat.

The NetCDF format SLC is read using a command such as:

par_SWOT_SLC
SWOT_L1B_HR_SLC_022_208_060R_20241008T185953_20241008T190004_PIC0_01.nc
20241008 SWOT.20241008.sch.dem SWOT.20241008.sch.dem_par

Here, in addition to the SLC (20241008_R_minus_y.slc and 20241008_R_plus_y.slc) files and their associated SLC parameter files (20241008_R_minus_y.slc.par and 20241008_R_plus_y.slc.par), the DEM section and associated DEM parameter file used in the data focusing are also written out.

The orbit state vectors cover a time span that does not extend much beyond the times corresponding to the data lines. This is problematic in the geocoding. We extend therefore the interval using *ORB_prop_SLC* with mode 2:

ORB_prop_SLC 20241008_R_minus_y.slc.par - 0.5 10 2

The SLC is in a skewed (= non-deskewed) geometry. We apply a deskewing using *SLC_deskew*. We manually set the near_range_slc parameter to the same value as the value indicated in the skewed SLC. The automatic selection of this parameter may be inappropriate in this case where the shortest slant ranges may not reach the terrain.

grep near_range_slc 20241008_R_minus_y.slc.par

SLC_deskew 20241008_R_minus_y.slc 20241008_R_minus_y.slc.par 20241008_RA.slc
20241008_RA.slc.par 0 0 5 1 1 900910

The SLC spectrum can be checked using

dismph_fft 20240111_RA.slc 4630 1 0 1. .35 128 3 0

Figure 1 shows the spectrum in an area near the image center.

Figure 1 SLC spectrum of the SWOT data. In the azimuth direction the spectrum is not centered due to a significantly non-zero Doppler Centroid. In the range direction, the spectrum does not seem to be clearly constrained, possibly related to the time-domain back-projection processing used to focus the data.

The backscatter values over land are quite low, so that signal noise becomes very relevant. To maintain a high spatial resolution while applying more spatial multi-looking we use *multi_look2*

multi_look2 20241008_RA.slc 20241008_RA.slc.par 20241008_RA.mli 20241008_RA.mli.par 1 5 3 15 0 2 7

The backscatter is shown in Figure 2. Notice that the backscattering over water (both oceans and inland water bodies) is (most of the time) very high at these low incidence angles. Over land (fields, forest) the backscatter is lower. Over water, there are typically small surface facets that point directly back at the sensor. Over land, small scale roughness and vegetation tends to scatter the Ka band signal away from the sensor, so “the rougher the surface the lower the backscatter” which is different from larger incidence angles.

At the very near range, the slant range seems to be shorter than the distance to the ground, so no surface return is obtained. At both the near range and the far range the contrast over land seems to be low, which is an indication that the backscatter from the target does not dominate over the system noise. Water surfaces can be recognized even in the far range because of their very high backscatter values. In the center of the image fields, urban areas, forests, rivers can be recognized quite well.

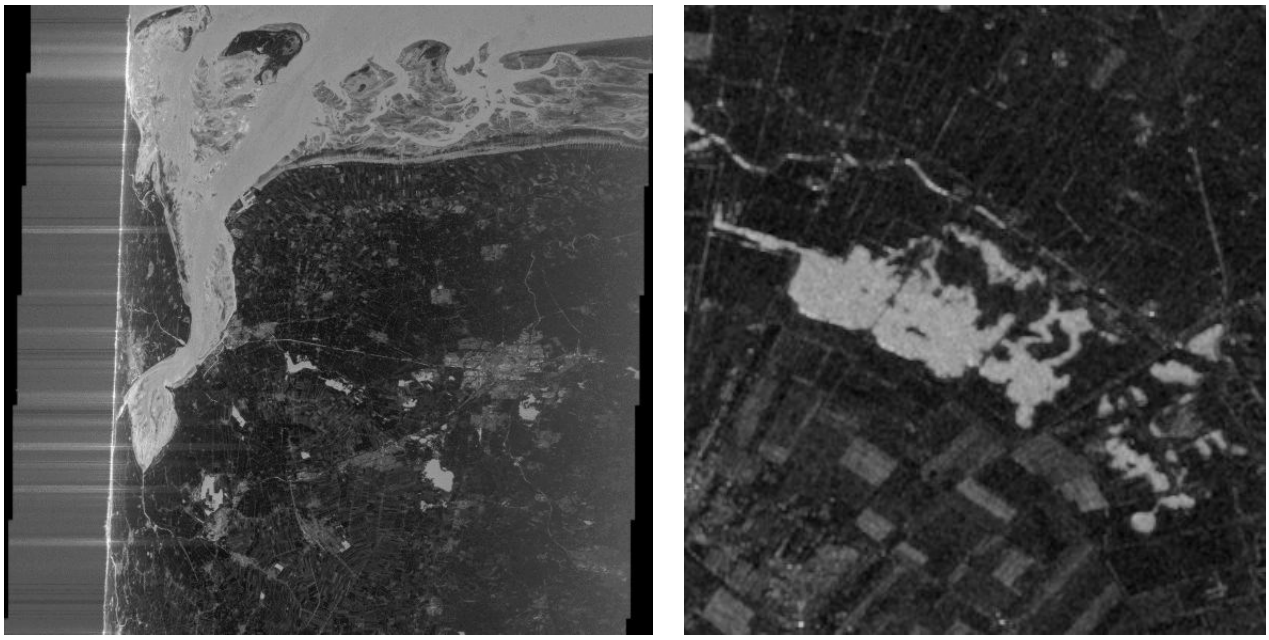

Figure 2 Right looking, descending orbit, SWOT KaRIn backscatter image over Groningen, NL The image to the left shows an overview over one acquisition, the image to the right a small section of it.

2.2. Imported DEM

The DEM heights used in the time-domain back-projection processing are provided with each SWOT KaRIn SLC. The reader program generates the related DEM and DEM parameter files. The projection used is SCH (Spherical Cross-track Height). This geometry is supported in the GAMMA Software. The SCH DEM can be transformed into other map projections using *dem_trans*. In Figure 3 the SRTM-based heights obtained with the SWOT data and the Copernicus 1" DEM heights are compared.

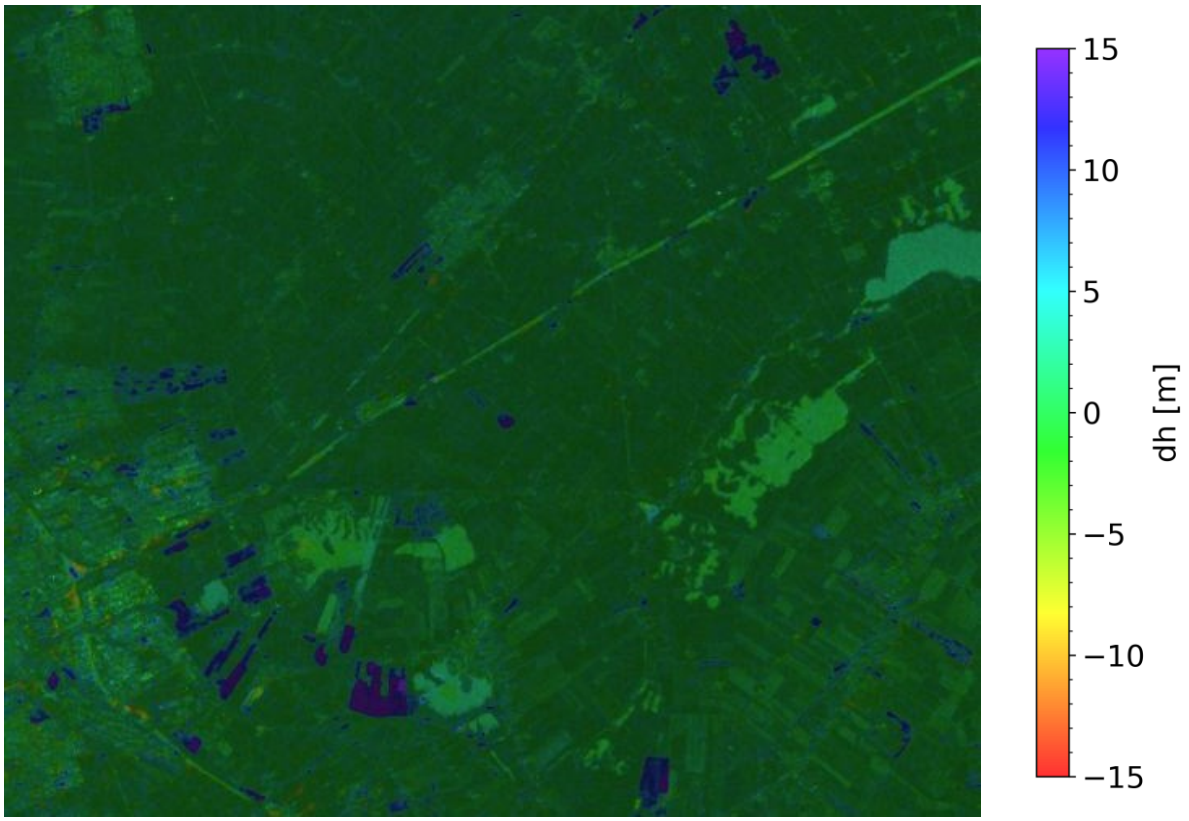

Figure 3 Difference between Copernicus 1" DEM and "SWOT data DEM" heights. The height differences correspond mainly to forested areas, where the Copernicus DEM heights tend to be about 10m to 20m higher than the SRTM DEM heights. Overall, the height differences are small. For inland water surfaces we observe differences of up to several meters. When determining relative height corrections, it is important to keep in mind what reference height is used.

2.3. Geocoding

The normal geocoding procedure using the Copernicus DEM as height reference, e.g. using *geocoding.py* with a refinement step, worked well. In spite of the flat terrain, the refinement was successful and the estimated offsets were small with good statistics. This confirms that the quality of the state vectors is high.

Layover is very significant at the very steep incidence angles used. At 3 deg. incidence angle a target such as a roof of a building or the top of a forest, located 20m above the flat horizontal ground, mixes with the ground surface pixels 370m away from it. Even in the very flat area around Groningen layover becomes therefore relevant. Figure 4 shows the geocoded backscatter image with and without the layover area removed. Furthermore, the data is masked to the center parts of the antenna, which corresponds to the area where the backscatter can more reasonably be used over land. In areas with more topographic variation the layover effects become much more severe (Figure 5).

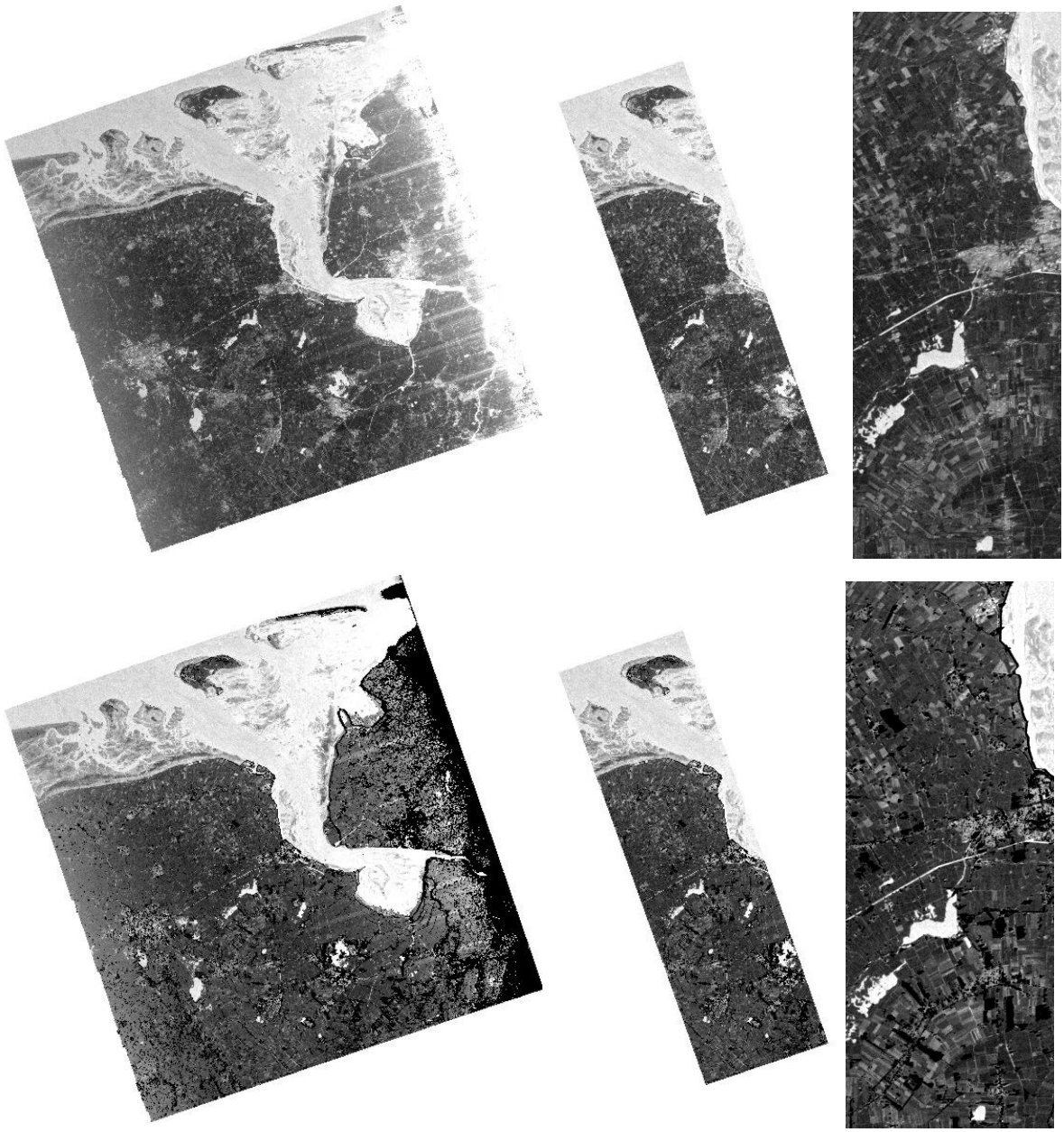

Figure 4 Geocoded SWOT backscatter over Groningen, NL. The top left image shows the geocoded image without masking. In the bottom left image, the layover/shadow area has been masked (is now black). In the top and bottom images in the center the coverage has been masked to the incidence angle range between 2.0 deg. and 3.5 deg., with and without layover/shadow masking. The images to the right show a small section of the images in the center at greater detail.

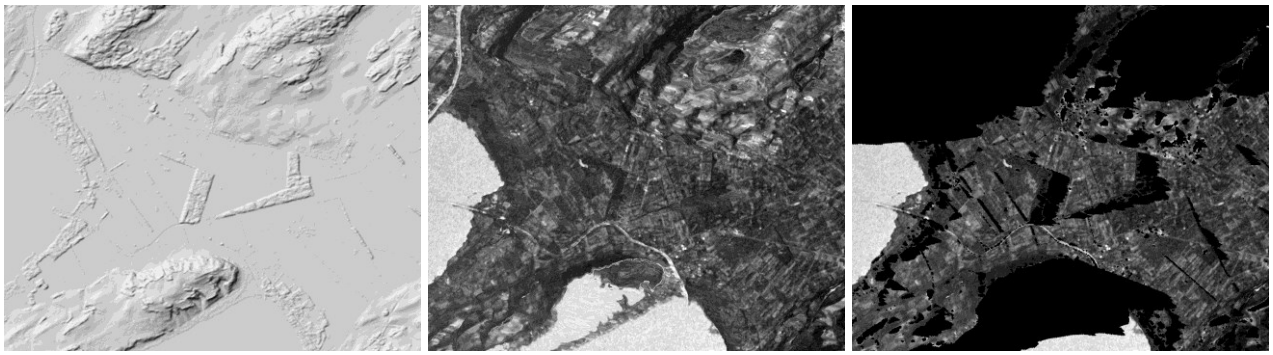

Figure 5 Section of geocoded SWOT backscatter over Ins, Switzerland. The image to the left shows the shaded relief of the area, the image in the center the geocoded SWOT backscatter without masking layover/shadow areas, and the image to the right shows the geocoded SWOT backscatter with masked layover/shadow areas.

3. SWOT DINSAR

3.1. Generation of single pass SWOT interferogram

Based on a monostatic – bistatic SWOT KaRIn SLC pair a single pass interferogram can be calculated. In the time-domain back-projection processing used to generate the SLCs the phase is already corrected for the orbital and topographic phase, using the SRTM-based DEM heights provided with the SLC. Consequently, the calculated interferogram corresponds to a differential interferogram with the topographic and orbital phase subtracted. Differential interferometric phases can be converted to height corrections relative to the used reference height. The SLCs are already co-registered.

The interferogram is calculated, starting from the deskewed SLC pair, using *SLC_intf2*:

SLC_intf2 20241008_RA.slc 20241008_RB.slc 20241008_RA.slc.par 20241008_RB.slc.par 20241008_RA.mli 20241008_RB.mli 20241008_RA.mli.par 20241008_RB.mli.par 20241008.RA_RB.int 20241008.RA_RB.cc 1 5 3 15 0 2

The complex valued interferogram and the coherence can be visualized using

rasmph_pwr 20241008.RA_RB.int 20241008_RA.mli 6164 1 - 1 1 rmg.cm 20241008.RA_RB.int 1. .35 24

ras_linear 20241008.RA_RB.cc 6164 1 - 1 1 0. 1. 0 gray.cm 20241008.RA_RB.cc.bmp 0

A section of the resulting images in slant range geometry, together with the layover/shadow masked backscatter image, is shown in Figure 6.

The interferometric phase can then be unwrapped either using *mcf* or using a direct conversion with *cpx_to_real* if the phase differences are smaller than half a phase cycle. To convert the unwrapped phases to height corrections relative to the reference DEM heights the program *dh_map_orb* is used. Besides the height corrections it also calculates the phase-to-height sensitivity – which varies for SWOT KaRIn between about 20m per phase cycle in near range and 60m per phase cycle in far range.

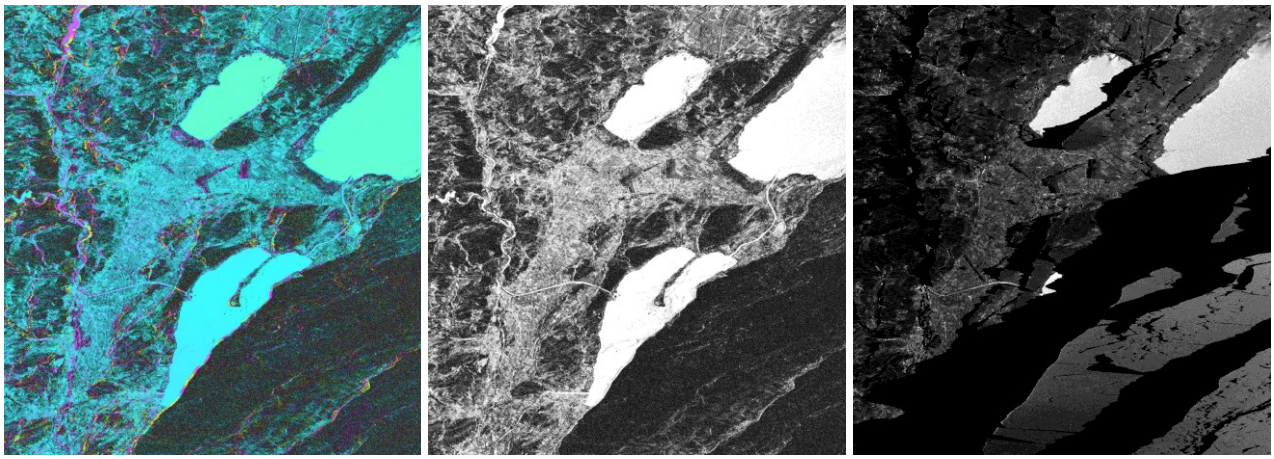

Figure 6 Section of the SWOT interferogram over Ins, Switzerland, on 2-Oct-2024 (left), the related coherence image (center), and the layover/shadow masked backscatter (right).

Over the lakes, the interferometric phase in slant range geometry looks smooth, in spite of the severe layover effects present. For the lake below the image center all except a very small section is affected by layover effects caused by the Jura mountains. Why is this possible? It helps that the backscatter over the lake is significantly higher than the backscatter over the mountain area. Furthermore, it is necessary that the reference height used in the focusing (and used to subtract the orbital and topographic phase) is smooth over the lake area.

Using our normal resampling procedure, the terrain height of a slant range pixel that is affected by layover is a combination of the heights of the terrain sections that contribute to this pixel – so a combination of the lake height and significantly larger heights of the nearby mountain area. As a result, the reference height obtained is strongly varying over the part of the lake affected by layover. So, obviously, a different resampling procedure was used to get the reference terrain height in slant range geometry.

DEM heights in SCH coordinates are provided with the SLC data. This data is organized in the ground-range direction. We think that the heights were resampled to the slant range geometry such that heights were only resampled if the related slant range was larger than the maximum of the previous slant range values of this ground-range line. In Figure 7, we compared this "increasing slant ranges" method for different situations with our normal procedure. With the "increasing slant ranges" method the reference height in slant range geometry remains at the lake height (in spite of the layover present). As long as the backscatter from the lake dominates over the other pixels contributing this is a reasonable choice that permits estimating the lake height from the interferometric phase. But you need to be aware that there are also cases where the lake surface is very smooth, so that the backscatter over the water become very low. In this case the scattering from the laid over mountain area dominates and here the lake height is not an appropriate reference height.

Alternatively, the selection criteria of the "increasing slant ranges" method can also be defined as "taking the lowest height". This criterion is equivalent – and it explains why the method is quite well suited for a sensor that has usually the highest backscatter values over water.

Using the "increasing slant ranges" method to transform the terrain height into the slant range geometry is not so much our attempt to get a better suited height but it is our attempt to get the height

that was actually used in the processing – and which is therefore the relevant reference height relative to which height corrections should be interpreted.

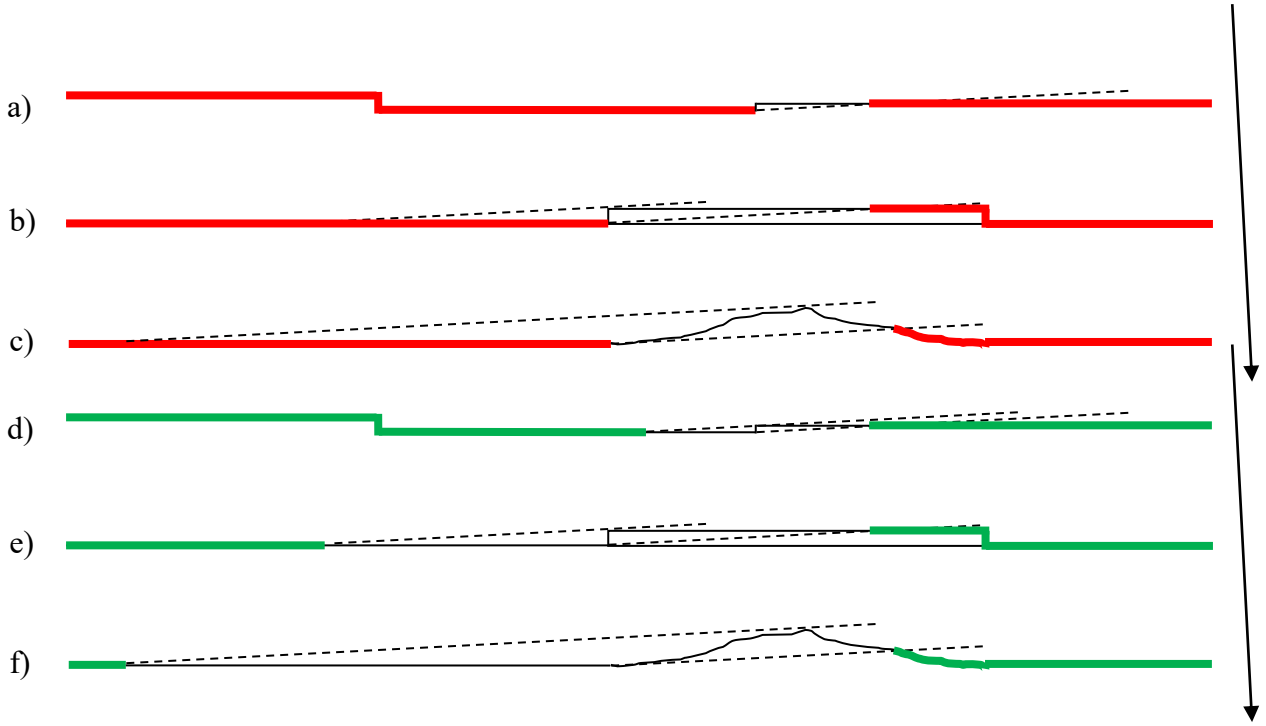

Figure 7 The graphs show the terrain height along a ground range line. The red lines in (a) to (c) show the heights used in the "increasing slant ranges" method, for an example of a water body (a), a forest or building (b), and a small hill (c). The heights in the sections without red line are not used. The slant range of the first pixel of the red line after the gap is slightly larger than the slant range of the pixel before the gap. The green lines in (d) to (f) show the heights used in our normal transformation method used, again for an example of a water body (d), a forest or building (e), and a small hill (f). The gaps between the two sections of the green lines are larger than with the "increasing slant ranges" method, because the section before the start of the laid over area that is affected by the layover process is also masked. Depending on the exact method used either gaps result in the height map in slant range geometry, or the heights corresponding to a mixture of the two or more sections contributing to a slant range pixel are combined.

3.2. Geocoding of SWOT data using the "increasing slant ranges" method

Above we discussed the transformation of terrain heights from the map (or ground-range) into the slant range geometry and we considered some advantages of the "increasing slant ranges" method. The same method, can also be used in the transformation of data from the slant range to the map geometry. In Figure 8 results using our normal geocoding procedure and results obtained using the "increasing slant ranges" method.

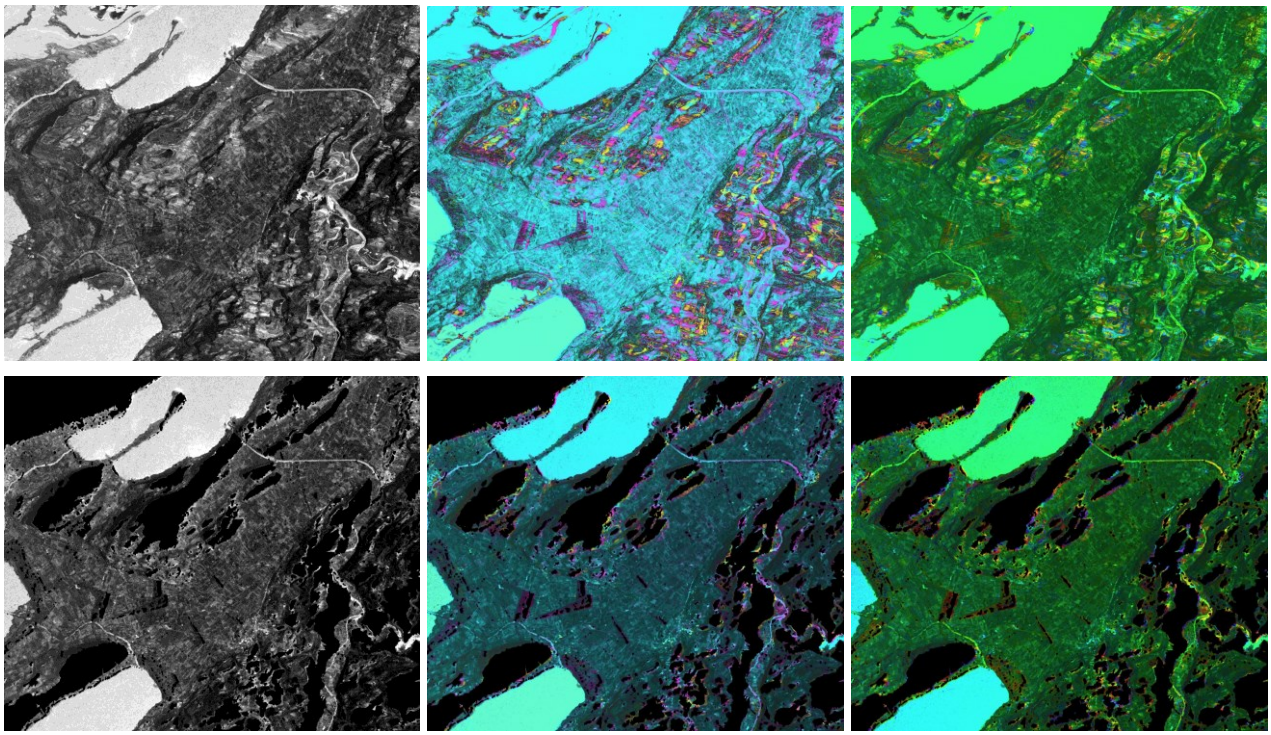

Figure 8 The SWOT backscatter (left), the single-pass interferogram (center) and height corrections (right, using a color scale between -15m (red), 0m (green), and 15m (blue)) estimated based on the unwrapped interferometric phase were geocoded into map coordinates using our normal geocoding procedure (top line) and using the "increasing slant ranges" method (bottom line).

With the "increasing slant ranges" method there are gaps in the coverage. With the normal geocoding method, the lake results are also visible in the corresponding layover areas on the nearby hills. Masking the layover/shadow areas, on the other hand, will result in much larger gaps, including more of the lake at the top of the section shown.

The height corrections over water bodies look very plausible. For two of the lakes partly shown in Figure 8 the reference height used in the SAR data focusing deviates from the actual lake height by about 5 meter and this is corrected with the determined height correction. We did not conduct a detailed validation of results over water as this is done elsewhere, as determining water heights is one of the key topics studied using the SWOT KaRIn instrument.

Over land, we find height corrections for forest areas. When carefully checking the SRTM-based reference heights that were used in the focusing, we found that the observed height corrections partly "undo" the forest height present in the height reference. Hence, it seems that the effective SWOT forest height is significantly smaller than the heights in the SRTM DEM. The same is true for the Copernicus DEM forest heights – which are even higher than the SRTM DEM forest heights. A possible explanation could be that contribution from the ground below the forest, caused by specular scattering, are a relevant fraction of the backscattering and maybe also having a higher coherence.

This should be different for buildings, as there are no gaps, and indeed we observe in data over the Camargue, plausible positive height corrections for new large industrial buildings (which are not present in the reference DEM height), as shown in Figure 9.

Height differences observed during low tide conditions may be of interest to monitor the terrain height in tidal flats. An example is shown in Figure 10.

Figure 9 Positive height corrections are observed for new industrial buildings in the Camargue, France. The height of these buildings is not present in the SRTM based height reference used in the SWOT data focusing.

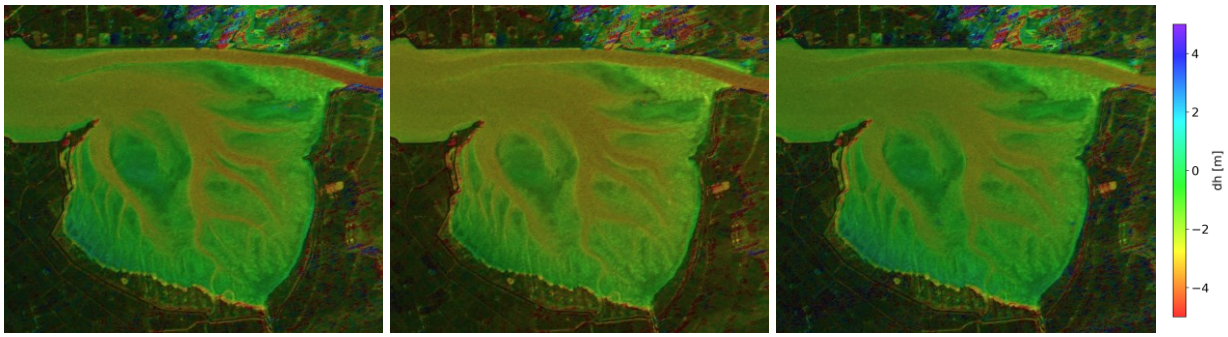

20231130 20240404 20241008

Figure 10 Height difference maps obtained in the tidal flats at the Dutch – German border, during low tides.

4. SWOT BACKSCATTER, COHERENCE, AND PHASE

4.1. SWOT backscatter and single-pass coherence over land

In the center of the swath the backscatter over land shows variation between different agricultural fields, forest, and other surfaces (urban, water bodies) indicating some potential for land-use applications such as crop monitoring, soil moisture monitoring, land-use classification etc.

In the very near range the geometry is significantly affected by layover effects. In addition, the backscatter over fields and forests is not much above the Noise Equivalent Sigma Zero (NESZ) level, resulting in reduced contrast. In the far range, the backscatter signal gets even lower, so that the signal levels fall below the noise level. Consequently, the backscatter can most reasonably be used in the center swath at incidence angles between about 2 deg. and 3.5 deg. (see Figure 4 above). An exception to this are water areas, which show higher backscatter also in the very near and far range.

Over water surfaces with a high backscatter level the single-pass coherence is typically high (> 0.9). Over other land targets the coherence depends strongly on the backscatter level. It seems that system noise is the dominant decorrelation mechanism. As a consequence the coherence does, unfortunately, not provide much complementary information.

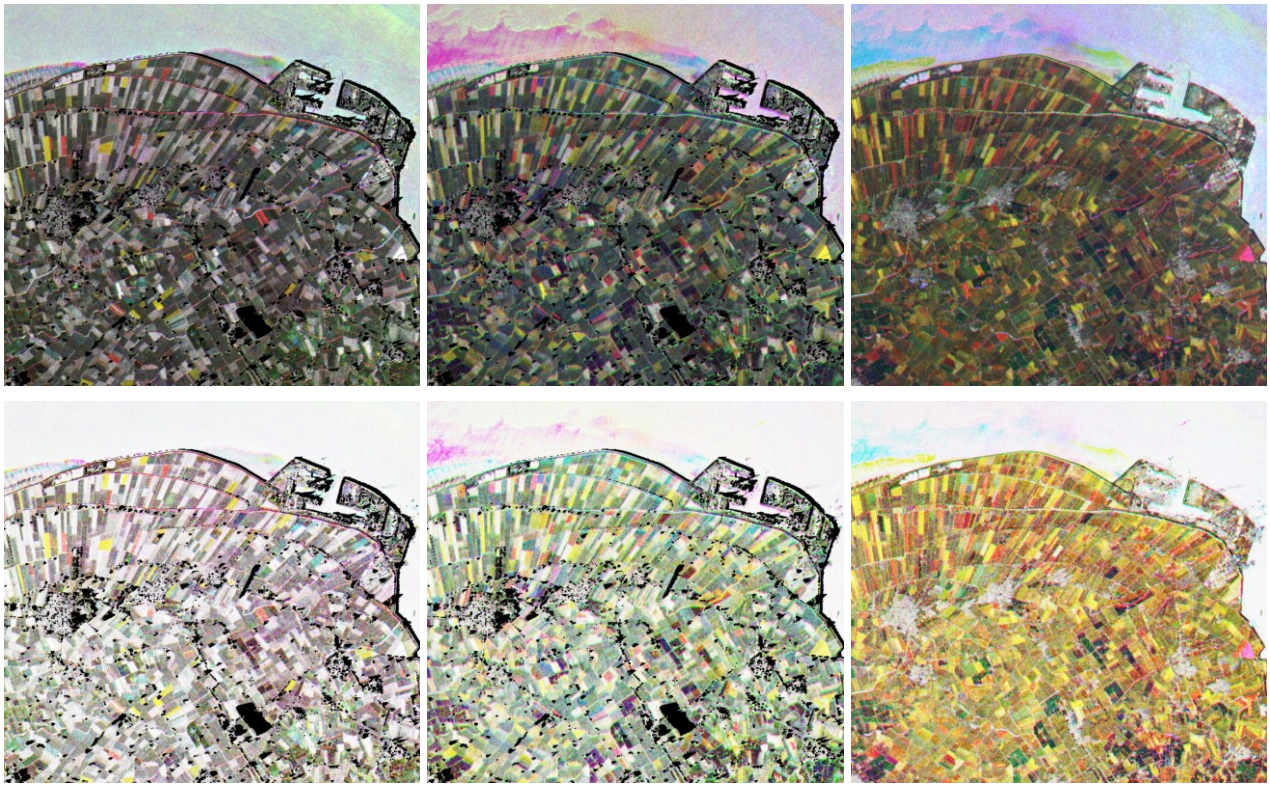

20240201.20240222.20240314 20240314.20240404.20240424 20240404_20240424_20240515

Figure 11 Multi-temporal SWOT backscatter (top) and SWOT single-pass coherence (bottom) composites over Groningen, NL. The three dates considered as red, green, and blue channel are indicated below the image.

Figure 11 shows multi-temporal composites of the SWOT backscatter and SWOT single-pass coherence for spring 2024. With increasing vegetation cover the backscatter and coherence decrease. Figure 12 shows an RGB composite of the temporal standard deviation of the coherence (red), the temporal standard deviation of the backscatter (green) and the temporal median of the backscatter (blue). The temporal median and standard deviation were calculated using the LAT programs *temp_lin_var, temp_log_var, multi_stat*.

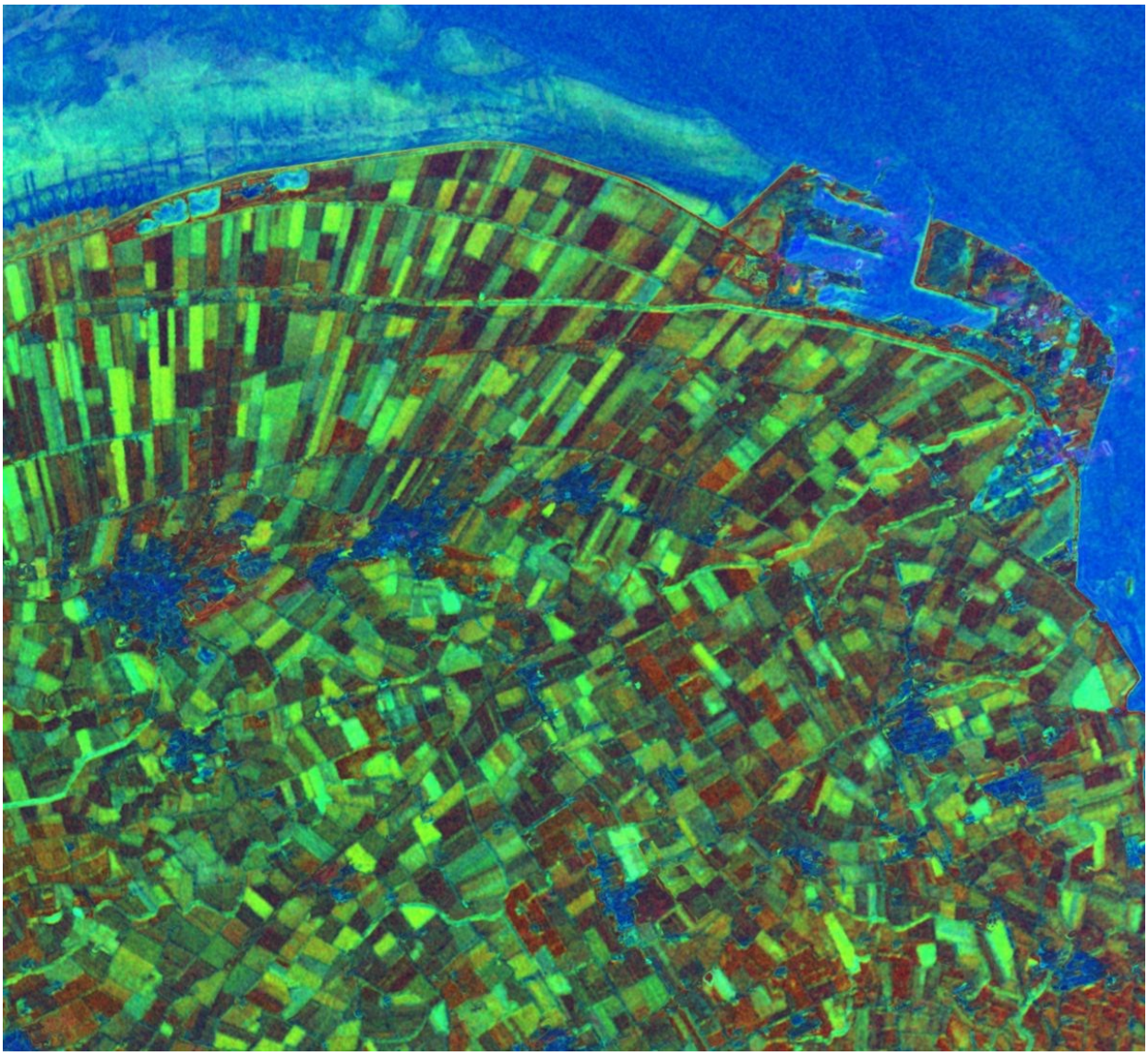

Figure 12 RGB composite of the temporal standard deviation of the coherence (red), the temporal standard deviation of the backscatter (green) and the temporal median of the backscatter (blue).

4.2. SWOT backscatter and height corrections over sea ice

To investigate the use of SWOT KaRIn SLC over sea ice a multi-seasonal stack of acquisitions over a section of the Gulf of Bothnia near Oulu, Finland was analyzed. The backscatter time-series obtained is shown in Figure 13. The formation of the sea ice is clearly visible. Then, in winter snow cover also plays an important role on the near-nadir viewing Ka-band backscattering. The height corrections relative to the SRTM-based height reference used in the back-projection processor, determined from the interferometric phase, and after subtracting a quadratic phase trend, are shown in Figure 14. According to the Finnish Meteorological Institute ice thickness is up to about 60cm, so the ice related elevation changes are < 10cm. Tidal maxima are about 3 meters apart.

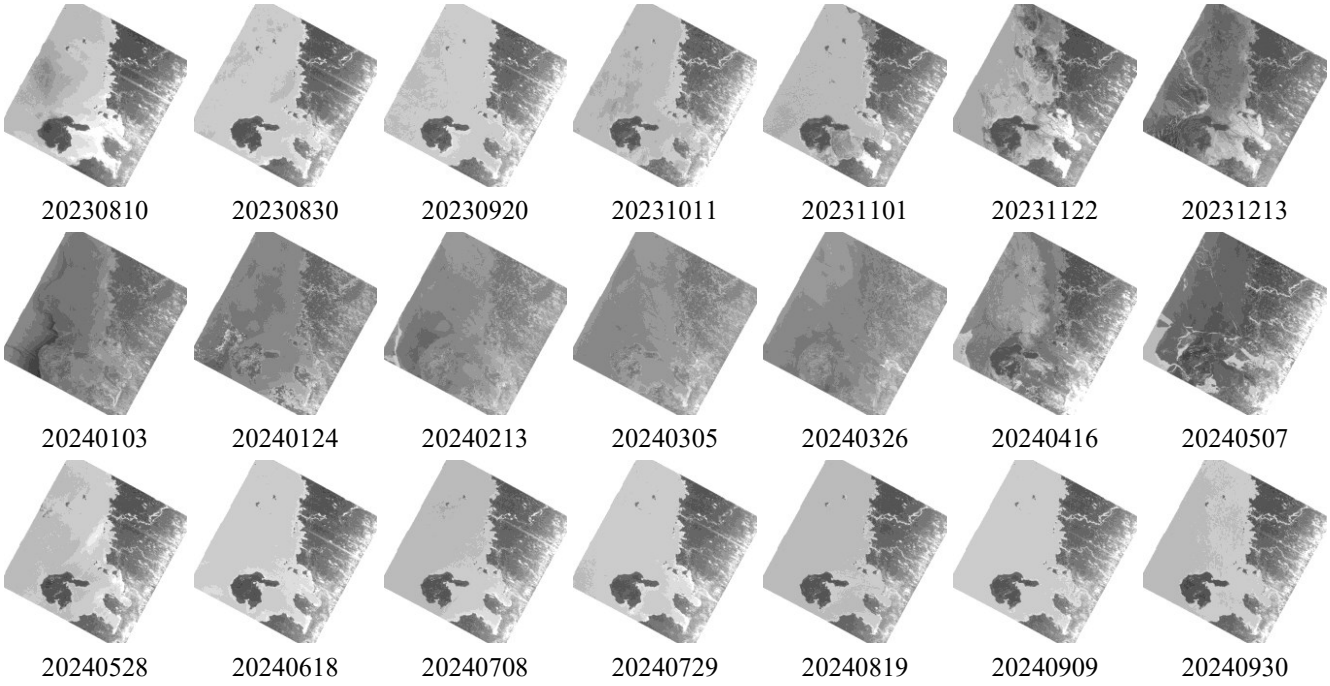

Figure 13 SWOT KaRIn backscatter time-series over the Gulf of Bothnia, near Oulu, Finland. First parts of the sea are frozen on 20231101. On 20231213 the section shown is more or less completely frozen. The ice disappears between 20240507 and 20240528. A closer look at the images reveals interesting details on the sea ice, snow cover, related processes, ice roads, etc.

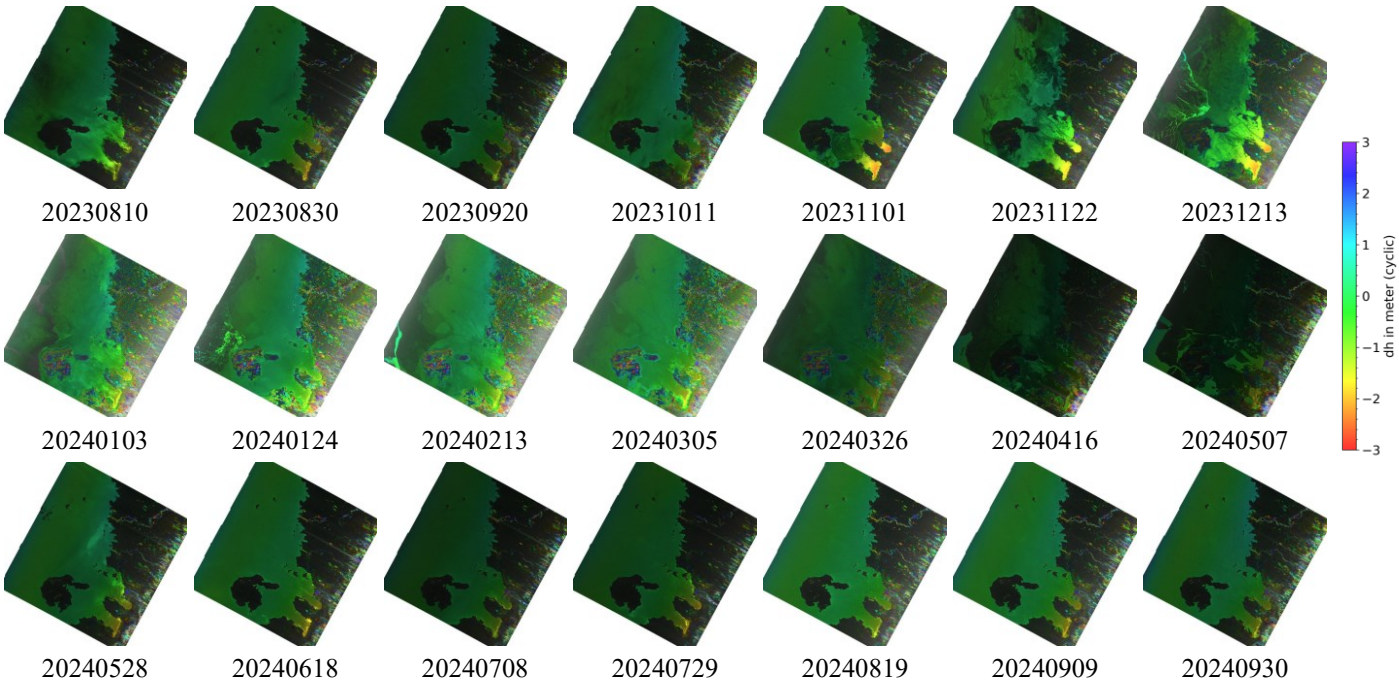

Figure 14 SWOT KaRIn relative height correction time-series over the Gulf of Bothnia, near Oulu, Finland.

5. ACKNOWLEDGMENT AND COPYRIGHTS

NASA JPL is acknowledged for providing access to the SWOT KaRIn SLC data used.